Open Veterinary Journal, (2024), Vol. 14(1): 416–427
ISSN: 2226-4485 (Print)
ISSN: 2218-6050 (Online)
Original Research
DOI: *10.5455/OVJ.2024.v14.i1.38*

Submitted: 01/10/2023 Accepted: 15/12/2023 Published: 31/01/2024

The ameliorative role of *Aloe vera*-loaded chitosan nanoparticles on *Staphylococcus aureus* induced acute lung injury: Targeting TLR/NF-κB signaling pathways

Mahran M. Abd El-Emam[1], Azza S. El-Demerdash[2*], Samar A. Abdo[1], Eman B. Abd-Elfatah[3], Marwa M. El-Sayed[4], Milad R. Qelliny[4], Zienab E. Eldin[5] and Ayman A. Shehata[3]

[1]*Department of Biochemistry and Molecular Biology, Faculty of Veterinary Medicine, Zagazig University, Zagazig, Egypt*
[2]*Laboratory of Biotechnology, Agriculture Research Center (ARC), Department of Microbiology, Animal Health Research Institute (AHRI), Zagazig, Egypt*
[3]*Department of Animal Medicine, Infectious Diseases, Faculty of Veterinary Medicine, Zagazig University, Zagazig, Egypt*
[4]*Department of Pharmaceutics, Faculty of Pharmacy, Minia University, Minia, Egypt*
[5]*Department of Materials Science and Nanotechnology, Faculty of Postgraduate Studies for Advanced Sciences, Beni-Suef University, Beni-Suef, Egypt*

ABSTRACT

Background: Acute lung injury (ALI) is a severe condition distinguished by inflammation and impaired gas exchange in the lungs. *Staphylococcus aureus,* a common bacterium, can cause ALI through its virulence factors. *Aloe vera* is a medicinal plant that has been traditionally used to treat a variety of illnesses due to its anti-inflammatory properties. Chitosan nanoparticles are biocompatible and totally biodegradable materials that have shown potential in drug delivery systems.

Aim: To explore the antibacterial activity of *Aloe vera*-loaded chitosan nanoparticles (AV-CS-NPs) against *S. aureus in vitro* and *in vivo* with advanced techniques.

Methods: The antibacterial efficacy of AV-CS-NPs was evaluated through a broth microdilution assay. In addition, the impact of AV-CS-NPs on *S. aureus*-induced ALI in rats was examined by analyzing the expression of genes linked to inflammation, oxidative stress, and apoptosis. Furthermore, rat lung tissue was scanned histologically. The rats were divided into three groups: control, ALI, and treatment with AV-CS-NPs.

Results: The AV-CS-NPs that were prepared exhibited clustered semispherical and spherical forms, having an average particle size of approximately 60 nm. These nanoparticles displayed a diverse structure with an uneven distribution of particle sizes. The maximum entrapment efficiency of 95.5% ± 1.25% was achieved. The obtained findings revealed that The minimum inhibitory concentration and minimum bactericidal concentration values were determined to be 5 and 10 ug/ml, respectively, indicating the potent bactericidal effect of the NPs. Also, *S. aureus* infected rats explored upregulation in the mRNA expression of *TLR2* and *TLR4* compared to healthy control groups. AV-CS-NP treatment reverses the case where there was repression in mRNA expression of *TLR2* and *TLR4* compared to *S. aureus*-treated rats.

Conclusion: These NPs can serve as potential candidates for the development of alternative antimicrobial agents.

Keywords: Acute lung injury, *Aloe vera*, Chitosan nanoparticles, NF-κB pathway, *S. aureus*.

Introduction

Acute lung injury (ALI) is a common and consequential medical condition characterized by respiratory failure and acute respiratory distress syndrome. It has a mortality rate of around 45% (Phua *et al.*, 2009; Ricart *et al.*, 2020; Yoshida *et al.*, 2022). Numerous clinical conditions, such as sepsis, pneumonia, trauma, and so on, may develop into ALI (Yao *et al.*, 2017). Microbial infections are considered to be the primary factor contributing to ALI (Dreyfuss and Ricard, 2005). One of the most contagious Gram-positive bacteria causing ALI is *Staphylococcus aureus* (Sy *et al.*, 2015). A *S. aureus* infection activates the host's immune system, causing inflammatory cells such as neutrophils and

***Corresponding Author:** Azza S. El-Demerdash. Laboratory of Biotechnology, Agriculture Research Center (ARC), Department of Microbiology, Animal Health Research Institute (AHRI), Zagazig, Egypt.
Email: *dr.azzasalah@yahoo.com; dr.azza@ahri.gov.eg*

macrophages to invade the body. This leads to the release of cytokines and chemokines, resulting in an uncontrolled and excessively large inflammatory response (Lowy, 1998; El-Demerdash *et al.*, 2023a). In the progression of *S. aureus* pathogenesis, peptidoglycans and lipoteichoic acids, two components of the cell wall, control inducing an inflammatory response, oxidative damage, and apoptosis by activation of toll-like receptors 2 (TLR2) (Zhu *et al.*, 2016). Pro-inflammatory cytokines are responsible for inducing oxidative stress, while the activation of TLR2 enhances the activity of caspases, potentially leading to apoptosis (Xing *et al.*, 2011; Ma *et al.*, 2019). Unfortunately, there is currently no effective treatment medicine or strategy for *S. aureus*-induced ALI, and the development of new therapeutic approaches to treat this injury is clearly necessary.

Aloe vera, a plant native to semi-tropical regions and belonging to the Liliaceae family, possesses a diverse array of applications within traditional medicine (Gamboa-Gómez *et al.*, 2015). Two substances are found in AV leaves. The leaf's inner side has a gel, and the outer layer of the inner layer, which comes before the external covering, has a bitter yellow juice. Glucomannan, a sugar material in AV, gives the gel 98.5% water content and viscosity (Moghaddasi, 2010). Among these substances are acemannan (boosts the immune system), bradykinin (reduces inflammation), magnesium lactate (soothes itching), and other calming and anti-inflammatory substances including sialic acid and anti-prostaglandins (Alemdar and Agaoglu, 2009). Research has uncovered the remarkable properties of AV, which contains phenolic compounds that exhibit remarkable abilities to combat inflammation and fight against harmful bacteria. About 200 bioactive substances, including vitamins, minerals, proteins, lipids, amino acids, and polysaccharides, are contained in AV gel (Abdul Qadir *et al.*, 2017).

A vital role of nanoparticles (NPs) has been and will continue to be played in a variety of disciplines including medicine, industry, agriculture, the environment, and food (Salem *et al.*, 2022). Recently, chitosan nanoparticles (CS-NPs), which are derived from applied NPs, have been employed extensively for medical applications such as medication carriers and cosmetics (Quispe *et al.*, 2021; Ali *et al.*, 2023). Chitosan demonstrates biocompatibility, chelating ability, and antibacterial properties when it comes to a diverse variety of Gram-positive and Gram-negative bacteria, as well as fungi (Kishen *et al.*, 2008). The substantial biofilm effectiveness of CS-NPs has been shown in earlier *in vitro* experiments (Silva *et al.*, 2013). *Aloe vera* gel has acquired many pharmacological properties through the integration of CS-NPs, which are quite interesting to pharmaceutical manufacturers (Bajer *et al.*, 2020). When CS-NPs and *Aloe vera* extract were combined, wound healing induced by microbial infections improved. The primary reason behind the demise of microbial cells is the electrostatic interaction between the positively charged amino groups of chitosan and the negatively charged elements on the cell wall (Ranjbar and Yousefi, 2018). Consequently, the aim of the present study was to determine the effect of *Aloe vera*-loaded chitosan nanoparticles (AV-CS-NPs) on *S. aureus*-induced ALI in rats. This was achieved through histological examination of rat lung tissue and analysis of the expression of genes associated with inflammation, apoptosis, and oxidative stress.

Materials and Methods

Materials

The chemicals, namely acetic acid, sodium tripolyphosphate (TPP), dimethyl sulfoxide, ethanol, and medium molecular weight chitosan (75 kDa) were procured from Sigma Aldrich Co. situated in St. Louis, MO. Fresh *Aloe vera* plant leaves were collected from a nearby plant nursery. *Staphylococcus aureus* (ATCC 25923 strain) was purchased from Thermo Fisher Specialty Diagnostics Ltd (Hampshire, UK). Analytical grade and high-purity chemicals and solvents were used throughout.

Animals

For our current research, we acquired thirty male Wistar albino rats from the Experimental Animals' Centre at Zagazig University's Faculty of Veterinary Medicine. These rats weighed between 160 and 170 g. The rats received a standard laboratory commercial feed, water, and 2 weeks of acclimation (at a temperature of around 25°C) before the experiment.

Preparation extracts of Aloe vera

The insides of freshly cut leaves were scraped out with a sterilized spatula, avoiding any green leafy remains. The collected inner parts were ground and then lyophilized using a freeze dryer (Labconco, Kansas, MO). The dried *Aloe vera* was combined with 200 ml of methanol and stirred on a shaker for 3 days at room temperature. After that, the methanol was collected and evaporated. The yield of *Aloe vera* alcohol extraction was then stored at 20°C for future use (Chandegara and Varshney, 2013).

Creation of AV-CS-NPs

The CS-NPs were synthesized by initiating the gelation process of a CS solution using TPP. The presence of positively charged amino groups within the CS-NPs facilitates their interaction with the negatively charged TPP, resulting in ionotropic gelation. A clear solution was formed when 0.2 g of chitosan was dissolved in an aqueous acetic acid solution (1% *v/v*) and then agitated at room temperature using a magnetic stirrer. The pH of the chitosan solution was increased to 4.8–5.0 using 1 M NaOH. We prepared a solution of sodium TPP in water by dissolving TPP in distilled water. The concentration of the solution was 2 mg/ml. Dropwise addition of TPP solution on chitosan solution at a ratio of 3:1 (*v/v*, chitosan: TPP) under magnetic stirring (1,000 rpm) at room temperature and sonication (20

minutes) (Hosni *et al.*, 2022). To guarantee optimal stability of the properties of the NPs and to provide the most effective protection for the drug, the chitosan particle dispersion was subjected to a process involving cooling, centrifugation at a speed of 14,000 revolutions per minute for a duration of 20 minutes, and subsequent lyophilization. To produce AV-CS-NPs, the above-mentioned technique was followed, but before adding TPP, AV was added to the CS solution at varying concentrations for 1 hour while stirring constantly. Then, add TPP to the AV-CS solution under magnetic stirring, sonication, centrifugation, and 24-hour freeze-drying.

Characterization of the prepared CS-NPs

Morphology study

Transmission electron microscopy (TEM) and field emission scanning electron microscopy (FESEM) are two advanced imaging assays used to analyze the structural properties of the synthesized CS-NPs. The CS-NPs were imaged using a high-resolution TEM instrument (Jeol JEM-100S, Japan) and a cutting-edge FESEM microscope (JSM-7800F, Japan). Regarding TEM, the samples were prepared by dispersion in ethanol through sonication for 15 minutes at 25°C. Before dropping onto the carbon-coated copper grids, they were dyed with phospho-tungstic acid, and allowing it to dry for further analysis. Regarding FESEM, the electron microscope was equipped with energy-dispersive X-ray microanalysis software and employed with a Philips-XL30 device for better visualization. The specimens were made by suspending the samples with deionized water in a ratio of 1:5 (*v/v*) at room temperature.

Particle size analysis

The polydispersity index (PDI) value, zeta potential, colloidal stability, and hydrodynamic diameter of AV-CS-NPs have been computed with photon correlation spectroscope or dynamic light scattering (DLS) of the ZS90 Zetasizer instrument (Malvern, United Kingdom). Instead of using distilled water, acetone was utilized to maintain the sample volume (1 ml) constant during the analysis. The zeta potential diversity was assessed within a distilled water dispersant having a 1.330 refractive index. The data investigations were conducted effortlessly using an automated system, ensuring accuracy with three repeated readings for every trial.

Entrapment efficiency percentage (EE%)

Using a UV-VIS spectrophotometer (CAR100, Germany), the concentration of unbound AV was to quantified at its maximum absorption wavelength of 220 nm to assess the efficiency of collecting AV. Centrifugation was performed for 45 minutes at 14,000 rpm and 4°C to separate the nano-formula sample from the supernatant. The AV EE% was computed using the following equation after estimating the free AV in the supernatant three times ($n = 3$):

$$EE\ \% = \frac{(\text{Total amount of aloe vera} - \text{free amount of } \textit{Aloe vera})}{(\text{Total amount of } \textit{Aloe vera})} \times 100 \quad (1).$$

In vitro evaluation of antibacterial activity

Evaluation of minimum inhibitory concentration (MIC)

The antibacterial efficacy of AV-CS-NPs and AV extract was examined using the traditional broth dilution method by observing the visible growth of microorganisms in the agar broth. The samples underwent a sequential dilution process twice, where the amounts ranged from 100 to 1 µg/ml. These dilutions were made using a bacterial concentration that had been adjusted to 10^8 colony-forming units (CFU)/ml, following the 0.5 McFarland's standard. The aim was to determine the MIC in brain heart infusion (BHI) broth. The control was placed in a broth that was inoculated with bacteria and incubated for a period of 24 hours at a temperature of 37°C. The term "MIC endpoint" refers to the concentration of the sample at which no discernible growth is observed in the tubes. To verify the MIC value, the level of cloudiness in the tubes was measured visually before and after the incubation process.

Determination of minimum bactericidal concentration (MBC)

Once the samples' MICs were identified, 50 µl portions were taken from each tube that showed no visible bacterial growth. These portions were then placed on BHI agar plates and incubated at 37°C for a period of 24 hours. An antimicrobial agent's MBC is the point at which 99.9% of the bacteria in a population are eliminated. The objective was achieved by examining the presence of bacteria on agar plates before and after incubation.

Experimental design

Thirty male Wistar rats were divided into three groups at random. *Staph aureus* strain (ATCC 25923) used in this study was previously isolated from mastitis cases in cattle and molecularly identified by the biotechnology unit, Animal Health Institute, Zagazig, Egypt. Tryptic soy broth (TSB) medium was used to culture *S. aureus* overnight at 37°C, and then re-incubated at a 10:1 ratio into a fresh TSB medium. The bacterial culture was harvested and suspended in phosphate-buffered saline (PBS) until it reached a concentration of 1×10^9 CFU per milliliter after reaching the logarithmic stage of growth. Rats were given 100 µl/10 g of chloral hydrate (4%) intraperitoneally as anesthesia to initiate a lung infection. Then, using a blunt-headed syringe, a solution containing 2×10^8 *S. aureus* CFU or an equivalent volume of PBS was carefully injected into the trachea (Zhang *et al.*, 2020). To uniformly disseminate the bacterial solution across both lungs, the mouse was maintained upright for 1 minute. The following groups of experimental rats were chosen at

random: (1) Control group: The rats were administered saline through an intraperitoneal injection before being infected with PBS; (2) *S. aureus* group: The rats received an intraperitoneal injection of saline solution 2 hours before being infected with *S. aureus*; (3) AV-CS-NPs + *S. aureus* group: rats were injected intraperitoneally with AV-CS-NPs (5 mg/kg) 2 hours before *S. aureus* infection (Zhang *et al.*, 2020).

A whole lung was gathered 12 hours following the *S. aureus* infection. A portion was utilized for lung histomorphology study, while another was used to analyze the gene expression utilizing real-time PCR (RT-PCR).

mRNA quantification using RT-PCR

The lung tissue was subjected to RNA extraction and purification using the QIAamp RNeasy Mini kit (Qiagen, Germany, GmbH, Cat. No. 74904) as per the manufacturer's instructions. The quantity of RNA was determined using a Nanodrop 8000 (Thermo Fisher Scientific). The primers utilized in this study were provided by Metabion (Germany) and can be found in Table 1. For each reaction, a 25 µl mixture was prepared, consisting of 10 µl of the 2X HERA SYBR® Green RT-qPCR Master Mix (Willowfort, Nottinghamshire, UK), 1 µl of RT Enzyme Mix (20X), 0.5 µl of each primer (20 pmol/ml), 3 µl of RNAse-free water, and 5 µl of RNA template. The reaction was carried out using a step-one RT-PCR machine. The reverse transcription process occurred at 50°C for 30 minutes, followed by denaturation of the cDNA at 94°C for 15 minutes. Subsequently, 40 cycles of PCR were performed, comprising of 95°C for 15 seconds and 60°C for 30 seconds for amplification. The amplification curves and Ct values were analyzed using Step 1 software. According to the "Ct" approach described by Yuan *et al.* (2006), the Ct value of each sample was compared with that of the positive control group to assess the variation of gene expression in the RNA of the different samples using the following ratio:

$2^{-\Delta\Delta Ct}$.

Table 1. Primer sequences used in RT-PCR.

Genes	Primer	Sequence (5′-3′)	References
Gpx	Forward	GGTGTTCCAGTGCGCAGAT	Al-Rejaie *et al.* 2013
	Reverse	AGGGCTTCTATATCGGGTTCGA	
IL-6	Forward	TCCTACCCCAACTTCCAATGCTC	Peinnequin *et al.* 2004
	Reverse	TTGGATGGTCTTGGTCCTTAGCC	
IL-1β	Forward	CACCTCTCAAGCAGAGCACAG	Peinnequin *et al.* 2004
	Reverse	GGGTTCCATGGTGAAGTCAAC	
TNF-α	Forward	AAATGGGCTCCCTCTCATCAGTTC	Peinnequin *et al.* 2004
	Reverse	TCTGCTTGGTGGTTTGCTACGAC	
IL-10	Forward	GCAGGACTTTAAGGGTTACTTGG	O'Bryan *et al.* 2005
	Reverse	GGGGAGAAATCGATGACAGC	
NF-κB	Forward	AATTGCCCCGGCAT	Habibi *et al.* 2016
	Reverse	TCCCGTAACCGCGTA	
Paraoxonase-1	Forward	TGAGAGCTTCTATGCCACAAATG	Al-Rejaie *et al.* 2013
	Reverse	CCATGACAGGCCCAAGTACA	
Sulfiredoxin-1	Forward	AATCCCCAACCCCTGACTTT	Al-Rejaie *et al.* 2013
	Reverse	TGAACTGACCAGTGGAGACACAGT	
IFNγ	Forward	GTCATCGAATCGCACCTGA	Rumbaugh *et al.* 2001
	Reverse	GTGCTGGATCTGTGGGTTG	
TLR2	Forward	GTACGCAGTGAGTGGTGCAAGT	Le Mandat Schultz *et al.* 2007
	Reverse	GGCCGCGTCATTGTTCTC	
TLR4	Forward	AATCCCTGCATAGAGGTACTTCCTAAT	Le Mandat Schultz *et al.* 2007
	Reverse	CTCAGATCTAGGTTCTTGGTTGAATAAG	
β-actin	Forward	CCTGCTTGCTGATCCACA	Patel *et al.* 2013
	Reverse	CTGACCGAGCGTGGCTAG	

Gpx: Glutathione peroxidase, IL-6: Interleukin-6, IL-1β: Interleukin-1 beta, IL-10: Interleukin-10, NF-κB: nuclear factor kappa beta, IFNγ: interferon gamma, TLR2: toll like receptor-2, TLR4: toll like receptor-4.

Histological examination of the rat lung

Rat lung specimens were procured and promptly immersed in a buffered neutral formalin solution containing 10% concentration for a duration of 48 hours. Subsequently, the samples underwent dehydration by gradually increasing the concentration of alcohol. They were then cleansed using xylene and finally embedded in paraffin. The tissue blocks encased in paraffin were cut into 5-µm-thick sections using a microtome (Leica RM 2155, England). After dewaxing, the sections were stained with hematoxylin and eosin (H&E) as described by Suvarna *et al*. (2018).

Statistical analysis

The statistical significance of the comparison between the three experimental groups was assessed using one-way ANOVA. Statistics were considered significant when *p*-values were less than 0.05. Version 9.5.1 of GraphPad Prism (GraphPad Software, San Diego, CA) was used to create each graph.

Ethical approval

The research protocol was reviewed and approved by the ethics committee of the Faculty of Veterinary Medicine, Zagazig University, Egypt, and all methods were performed according to the relevant guidelines and regulations (approval number: ZU-IACUC/2/F/316/2023). The investigation was carried out in accordance with the guidelines set forth by ARRIVE, ensuring compliance with the recommended protocols and procedures.

Results

Characterization of AV-CS-NPs and surface morphology

Regarding ultrastructural analysis, to examine the morphology of the prepared NPs, TEM is utilized. The AV-CS-NPs generated exhibited aggregated semispherical and spherical shapes, with an uneven distribution of particle size and an average particle size of approximately 60 nm, as observed through transmission microscopy (Fig. 1). The SEM image revealed a complex network of AV-CS-NPs with wide pores and surface discontinuities. In addition, the AV-CS-NPs figure showed irregularity, roughness, and nonhomogeneity in the surface texture as well as straps and shrinkage. The preparation process, which involves combining two aqueous phases-one containing polymer CS and the other poly-anion TPP-to form a complex, maybe the cause of this discrepancy (Fig. 2).

Mean particle size diameter and zeta potential measurements

The size distribution of the formulated AV-CS-NPs was analyzed using the DLS technique, specifically the intensity distribution method. Both the intensity distribution and cumulant fit sizes showed similar results, indicating consistency. The hydrodynamic diameter size distribution of the synthesized formula nanoparticles had an average value of 290 nm. A broad peak width of the distribution was indicated by the PDI value (0.208), indicating a heterogeneous size distribution. A high signal-to-noise ratio was suggested by the intercept value (0.909). In comparison to what the TEM revealed, the hydrodynamic diameter size dispersion of AV-CS-NPs was a little larger. By measuring the zeta potential, the surface charge of the prepared formula AV-CS-NPs was estimated. The results showed that the zeta potential of the prepared AV-CS-NPs was found to be −19 mV. It is widely acknowledged that a zeta potential measurement exceeding 30 mV is deemed adequate to generate a repulsive force capable of preventing particle aggregation. The repulsion observed between particles signifies a low zeta potential value,

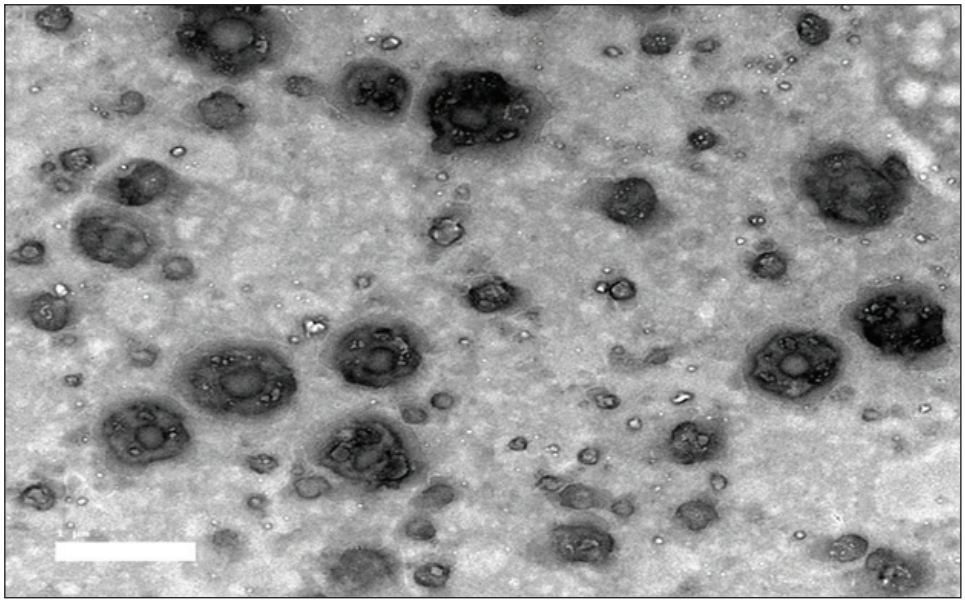

Fig. 1. TEM image of AV-CS-NPs.

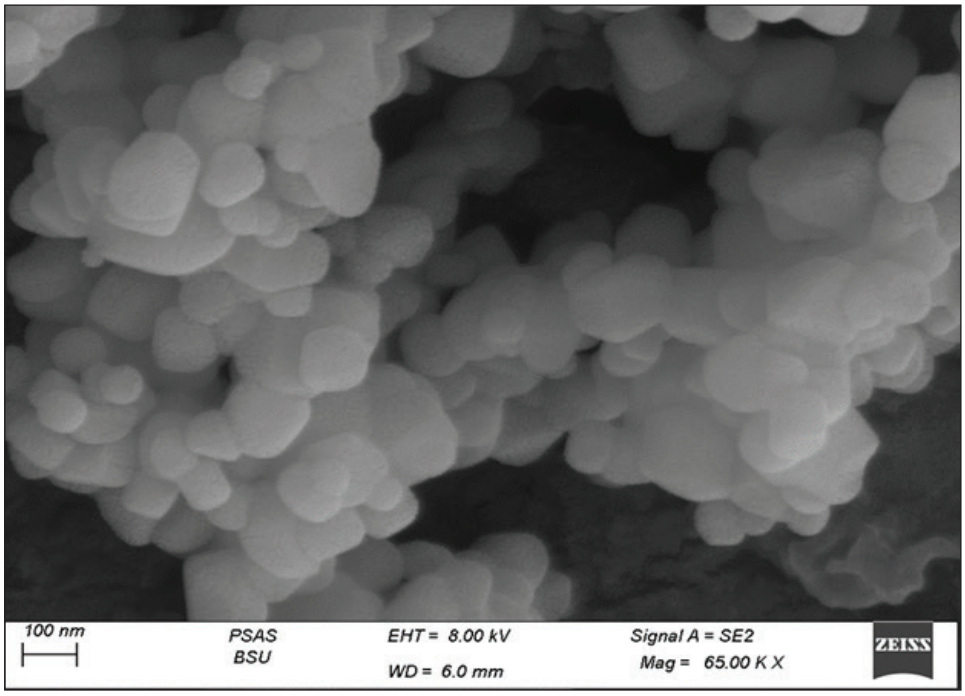

Fig. 2. SEM image of AV-CS-NPs.

indicating reduced physical stability and an increased likelihood of chemical or electrical interactions among the components. This was confirmed by the aggregated particles with the SEM image (Fig. 1B).

In vitro entrapment efficiency of Aloe vera into CS-NPs

The results indicated that at the given circumstances (CS: TTP, 3:1) at pH 4.8–5.0, the highest entrapment efficiency of *Aloe vera* into CS-NPs (95.5% 1.25%) was achieved.

In vitro evaluation of antibacterial activity of AV-CS-NPs

The MIC and MBC of AV-CS-NPs against *S. aureus* were determined to be 5 and 10 ug/ml, respectively. Typically, CS-NPs exhibit bactericidal or bacteriostatic properties. When the MBC to MIC ratio is small (less than 4), a drug is considered bactericidal, indicating that it can effectively eliminate 99.9% of the exposed organisms by achieving appropriate drug concentrations. Therefore, AV-CS-NPS can have potential bactericidal activity.

Alterations in Gpx, paraoxonase-1 and sulfiredoxin-1 mRNA expression levels following AV-CS-NPs administration

The study investigated the impact of the mRNA expression level of genes associated with the regulation of reactive oxygen species (ROS) accumulation within cells, including Gpx, paraoxonase-1, and Sulfiredoxin-1. Our data revealed that *S. aureus* rat group showed an increase in mRNA expression of paraoxonase-1 and Sulfiredoxin-1, and this upregulation was accompanied by a substantial decrease in the relative mRNA expression of antioxidant protein-associated genes such as *Gpx* compared to healthy control groups. However, AV-CS-NPs treatment reverses the case where there was repression in mRNA expression of paraoxonase-1 and Sulfiredoxin-1 and a significant elevation in *Gpx* relative mRNA gene expression (Fig. 3A–C).

Effects of AV-CS-NPs on the expression of inflammatory genes in lung tissue treated with S. aureus

This study was interested in investigating whether the regulatory mechanism of AV-CS-NPs treatment was associated with a change in the inflammatory genetic signature associated with ALI derived from *S. aureus* treatment (Fig. 4A–F). To address this issue, the inflammatory-related mRNA expression of the lung in *S. aureus* rat group treated with AV-CS-NPs was analyzed compared to the group treated with *S. aureus* alone. The results obtained showed that the lung of the *S. aureus* rat group treated with AV-CS-NPs had a significant decrease in the mRNA expression of genes associated with the pro-inflammatory signature, including IL-1β, TNF-α, IFN-γ, NF-κB, and IL-6 compared to the lung of rat group treated with *S. aureus* alone. However, pretreatment with AV-CS-NPs resulted in a prominent increase in the level of mRNA of the anti-inflammatory cytokine IL-10 when compared to *S. aureus* group.

Effects of AV-CS-NPs on TLR2 and TLR4 gene expressions in lung tissue treated with S. aureus

The obtained data revealed that *S. aureus* rat group exhibited upregulation in the mRNA expression of TLR2 and TLR4 compared to healthy control groups. AV-CS-NPs treatment reverses the case where there was repression in mRNA expression of TLR2 and TLR4 compared to *S. aureus* treated rats (Fig. 5A and B).

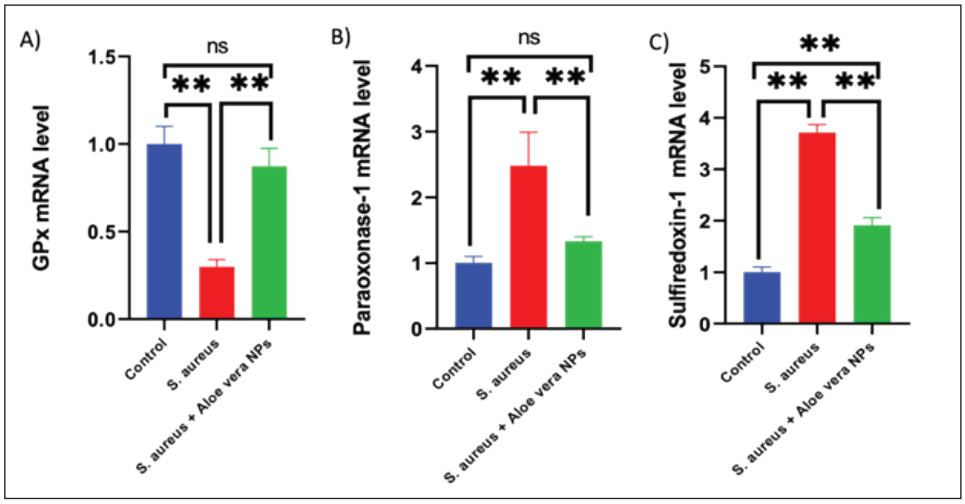

Fig. 3. Effect of AV-CS-NPs on mRNA level of antioxidants-related genes in lung tissues of staph *aureus* (*S. aureus*)-inoculated rats. (A) GPX; (B) Paraoxonase-1; (C) Sulfiredoxin-1. Data are presented as the mean ± SD of five rats from each group. $^{**}p < 0.01$ vs. control group. $^{*}p < 0.05$ versus control group.

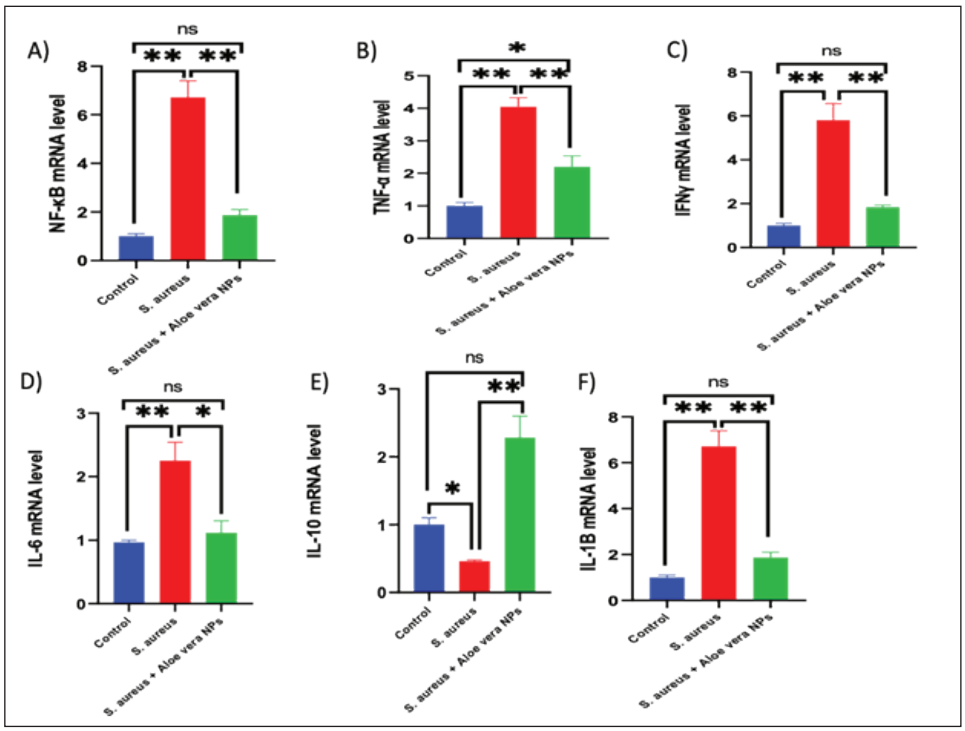

Fig. 4. Effect of AV-CS-NPs on mRNA level of inflammatory-related genes in lung tissues of staph *aureus* (*S. aureus*)-inoculated rats. (A) IL-1β; (B) TNF-α; (C) IFN-γ; (D) IL-6; (E) IL-10; and (F) NF-κB. Data are presented as the mean ± SD of five rats from each group. $^{**}p < 0.01$ versus control group. $^{*}p < 0.05$ versus control group.

Morphological changes of the lung tissues

Next, the effect of AV-CS-NPs injection on lung histology was examined after administration of *S. aureus*. The lungs of the control rat group showed normal structures of bronchi, bronchioles, alveolar epithelium, and pulmonary vasculatures (Fig. 6A). On the contrary, the *S. aureus*-treated group exhibited pneumonic areas alternated with emphysematous areas. The pneumonic areas showed impacted alveolar lumina with different leukocytic infiltrates. Some

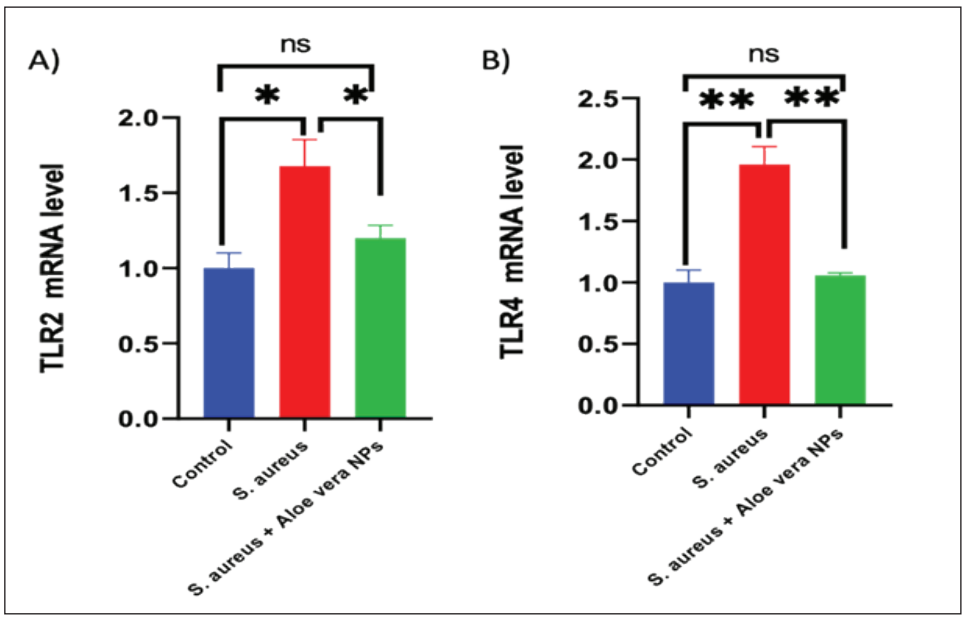

Fig. 5. Effect of AV-CS-NPs on *TLR2* and *TLR4* mRNA expression level in lung tissues of staph *aureus* (*S. aureus*)-inoculated rats. Data are presented as the mean ± SD of five rats from each group. $^{**}p < 0.01$ versus control group. $^{*}p < 0.05$ versus control group.

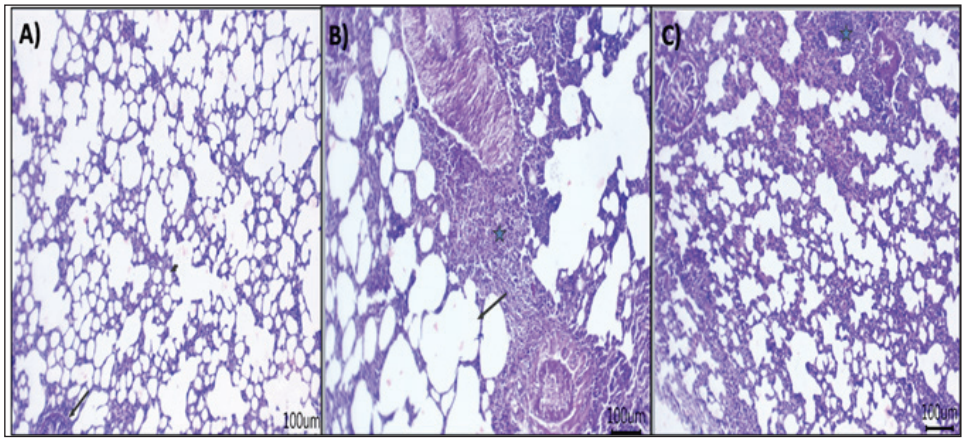

Fig. 6. Photomicrograph of H&E stained section from experimental groups: (A) control group: lung tissue showing normal structures of bronchiole and alveoli, (B) *S. aureus* group: lung tissue showing necrotic and desquamated lining epithelium of bronchiole leaving the denuded surface with inflammatory cells aggregates within bronchiolar wall mainly eosinophils, (C) AV-CS-NPs + *S. aureus* group: lung tissue revealed maintain structures, but perivascular inflammatory cells aggregates (star) and dilated perialveolar capillaries were also seen in some examined fields. Scale bar 100 µm.

bronchioles showed necrotic bronchiolitis which is represented by necrotic and desquamated lining epithelium leaving a denuded surface. Moreover, inflammatory cells aggregate within the bronchiolar wall and were also seen primarily as eosinophils and neutrophils (Fig. 6B). These pathological findings were improved after AV-CS-NPs treatment. Most of the pulmonary tissue showed maintained structures upon pretreatment with AV-CS-NPs (Fig. 5C). However, perivascular inflammatory cells aggregate (star) and dilated perialveolar capillaries were also seen in some examined fields (Fig. 6C).

Discussion

Microbial infections are a major problem all around the world (Ijaz *et al.*, 2018). When the human body is infected with *S. aureus*, it initiates an immediate inflammatory reaction. This response serves to eliminate the invading

pathogens, repair any damaged tissues, and ultimately reinstate a state of balance and stability within the body (Pollitt *et al.*, 2018). In contrast, an overabundance or unregulated occurrence of inflammation can lead to or exacerbate harm to tissues and organs (Lin *et al.*, 2018). Currently, glucocorticoids and nonsteroidal anti-inflammatory drugs (NSAIDs) are widely employed in pharmaceuticals. However, it is important to note that prolonged use of glucocorticoids can have significant detrimental impacts on the body. These adverse effects include reducing the body's ability to combat harmful microbes, causing osteoporosis, epilepsy, and various other complications (Oray *et al.*, 2016). Nonselective cyclooxygenase (COX) inhibitors can lead to significant complications in the form of gastric ulcers when used in conjunction with nonsteroidal NSAIDs. Conversely, selective COX-2 inhibitors pose an elevated threat to cardiovascular disease (Wong *et al.*, 2005). Finding new treatments for *S. aureus* infections is crucial due to the detrimental impacts of glucocorticoids and nonsteroidal anti-inflammatory medications. Recent research indicates that traditional Chinese medicines offer promising results in alleviating *S. aureus*-induced inflammation and providing protection against infections (Jiang *et al.*, 2017). In this work, the anti-inflammatory and antioxidant efficacy of AV-CS-NPs in *S. aureus*-induced ALI in rats was demonstrated. Pro-inflammatory cytokines such as IL-1, TNF-, IFN-, IL-6, and NF-κB were suppressed by AV-CS-NPs due to repression of the TLR4/NF-κB signaling pathway. Furthermore, AV-CS-NPs reduced ROS accumulation, which was linked to the overexpression of *Gpx* and the downregulation of paraoxonase-1 and Sulfiredoxin-1.

TLR2 and *TLR4* are two highly studied receptors that control the phagocytic death of Gram-positive and Gram-negative bacteria (Prince *et al.*, 2011). Previous research supports the concept that *TLR2* and *TLR4* play an essential role in the early inflammation caused by *S. aureus* (Wang *et al.*, 2015). This research aimed to investigate the gene expression analysis of the *TLR2* and *TLR4* signaling pathways using qRT-PCR. The NF-κB signaling pathways are widely recognized as crucial pathways involved in various essential functions, including immunological processes, cell survival, and inflammation (Lee *et al.*, 2010). The triggering NF-κB signaling pathway was characterized by the release of a large number of proinflammatory cytokines. Our study showed that *S. aureus* can activate the TLR signaling pathway. In addition, the expression of genes related to inflammation, such as IL-1β, TNF-α, IFN-γ, NF-κB, and IL-6, showed a significant increase in *S. aureus*. Conversely, the presence of the anti-inflammatory cytokine IL-10 was noticeably reduced, suggesting a strong inflammatory reaction. The results provide evidence that AV-CS-NPs may safeguard the respiratory system against *S. aureus*-induced harm by decreasing the expression of inflammatory cytokines and simultaneously enhancing the expression of anti-inflammatory cytokines. The results obtained were in alignment with Yahya *et al.* (2022), Cherukuri *et al.* (2022), and El-Demerdash *et al.* (2023b). Furthermore, the impact of AV-CS-NPs on TLR signaling is primarily controlled by *TLR2* and *TLR4* gene expression.

To evaluate the anti-oxidant efficacy of AV-CS-NPs, we investigated the effect of AV-CS-NPs on Gpx, paraoxonase-1, and Sulfiredoxin-1. Antioxidant enzymes are believed to be the first line of defense against oxidative damage in biological macromolecules. *GPx* acts to scavenge and break down excess hydroperoxides such as H_2O_2, which may be present under oxidative stress (Deitrich and Erwin, 1995). Sulfiredoxin1 (*Srxn1*) is a member of the sulfiredoxin family, which is a major component of redox signaling and regulates several physiological functions (Zhou *et al.*, 2015). The primary function of Srxn1 is to decrease the levels of peroxiredoxin hyper oxidation and hinder the excessive production of ROS. This crucial role serves to safeguard cells from the harmful effects of oxidative damage (Findlay *et al.*, 2005). The *PONs* family is composed of three genes, namely *PON1, PON2,* and *PON3*. These genes encode enzymes that possess the ability to break down organophosphate chemicals. In addition, they play a crucial role in processes related to inflammation and oxidative stress (Sokołowska *et al.*, 2005). The present data showed that AV-CS-NPs treatment repressed the mRNA expression of paraoxonase-1 and Sulfiredoxin-1 and a significant elevation in *Gpx* relative mRNA gene expression compared to *S. aureus* infected group. The findings acquired affirm the excellent antioxidant capabilities of *Aloe vera* when administered, which are consistent with various previously documented studies (Reza Nazifi *et al.*, 2019; Hossen *et al.*, 2022; Solaberrieta *et al.*, 2022). In addition, the application of AV-CS-NPs was found to diminish the structural harm to the lungs caused by *S. aureus*, as observed through H&E staining. These findings provide evidence that AV-CS-NPs effectively shield rats from the development of ALI induced by *S. aureus*.

Conclusion

The aim of this study was to develop AV-CS-NPs to achieve significant improvement in the efficiency of antibacterial activity of *Aloe vera* against *S. aureus*-induced ALI. Using the ionotropic gelation technique and TPP as a cross-linker, AV-CS-NPs were successfully produced. AV-CS-NPs displayed potent antioxidant, anti-inflammatory, and antibacterial activity in *S. aureus* infected rats by targeting the TLR pathway. The findings suggest that AV-CS-NPs possess potential therapeutic effects in reducing lung injury induced by *S. aureus*. The anti-inflammatory properties of *Aloe vera*, combined with the drug delivery capabilities of CS-NPs, may contribute to the observed amelioration of ALI.

Acknowledgment

Not applicable.

Authors' contributions

All authors participated in the conception of the study; MMA, ASE-D, and AAS contributed to the conception, design of the study, and conduction of the laboratory works. MME and FMM drafted the manuscript, analyzed the data, and revised the paper. The final iteration of the manuscript was read and endorsed by all the authors.

Conflict of interest

The authors have no competing interests to declare.

Funding

The authors did not receive any monetary assistance for conducting, writing, and/or publishing this article.

Data availability

The manuscript comprises all the data that has been utilized.

References

Abdul Qadir, M., Shahzadi, S.K., Bashir, A., Munir, A. and Shahzad, S. 2017. Evaluation of phenolic compounds and antioxidant and antimicrobial activities of some common herbs. Int. J. Anal. Chem. 2017, 3475738.

Alemdar, S. and Agaoglu, S. 2009. Investigation of *in vitro* antimicrobial activity of *Aloe vera* juice. J. Anim. Vet. Adv. 8(1), 99–102.

Ali, N.M., Mohamed, G.A.E. and El-Demerdash, A.S. 2023. Impact of oral administration of chitosan—nanoparticles on oxidative stress index and gut microbiota of heat stressed broilers. J. Adv. Vet. Res. 13(6), 997–1003

Al-Rejaie, S.S., Aleisa, A.M., Sayed-Ahmed, M.M., Al-Shabanah, O.A., Abuohashish, H.M., Ahmed, M.M. and Hafez, M.M. 2013. Protective effect of rutin on the antioxidant genes expression in hypercholestrolemic male Westar rat. BMC. Complement. Altern. Med. 13(1), 1–9.

Bajer, D., Janczak, K. and Bajer, K. 2020. Novel starch/chitosan/*Aloe vera* composites as promising biopackaging materials. J. Polym. Environ. 28(3), 1021–1039.

Chandegara, V.K. and Varshney, A.K. 2013. *Aloe vera* L. processing and products: a review. Int. J. Med. Aromat. Plants. 3(4), 492–506.

Cherukuri, S., Thiruppathi, M. and Vuppalapati, L. 2022. Formulation and optimization of novel dexibuprofen-*Aloe vera* deformable emulgels for enhanced anti-inflammatory activity. J. Drug. Deliv. 69, 103171.

Deitrich, R.A. and Erwin, V.G. 1995. Pharmacological effects of ethanol on the nervous system. Vol. 32. Boca Raton, FL: CRC Press.

Dreyfuss, D. and Ricard, J.D. 2005. Acute lung injury and bacterial infection. Clin. Chest. Med. 26(1), 105–112.

El-Demerdash, A.S., Bakry, N.R., Aggour, M.G., Elmasry, S.S., Mowafy, R.E. and Erfan, A. 2023a. Bovine mastitis in Egypt: bacterial etiology and evaluation of diagnostic biomarkers. Int. J. Vet. Sci. 12, 60–69.

El-Demerdash, A.S., Mohamady, S.N., Megahed, H.M. and Ali, N.M. 2023b. Evaluation of gene expression related to immunity, apoptosis, and gut integrity that underlies Artemisia's therapeutic effects in necrotic enteritis-challenged broilers. 3 Biotech. 13(6), 181.

Findlay, V.J., Tapiero, H. and Townsend, D.M. 2005. Sulfiredoxin: a potential therapeutic agent? Biomed. Pharmacother. 59(7), 374–379.

Gamboa-Gómez, C.I., Rocha-Guzmán, N.E., Gallegos-Infante, J.A., Moreno-Jiménez, M.R., Vázquez-Cabral, B.D. and González-Laredo, R.F. 2015. Plants with potential use on obesity and its complications. EXCLI. J. 14, 809.

Habibi, F., Soufi, F.G., Ghiasi, R., Khamaneh, A.M. and Alipour, M.R. 2016. Alteration in inflammation-related miR-146a expression in *NF-KB* signaling pathway in diabetic rat hippocampus. Adv. Pharm. Bull. 6(1), 99.

Hosni, A., Abdel-Moneim, A., Hussien, M., Zanaty, M.I., Eldin, Z.E. and El-Shahawy, A.A. 2022. Therapeutic significance of thymoquinone-loaded chitosan nanoparticles on streptozotocin/nicotinamide-induced diabetic rats: *in vitro* and *in vivo* functional analysis. Int. J. Biol. Macromol. 221, 1415–1427.

Hossen, M.M., Hossain, M.L., Mitra, K., Hossain, B., Bithi, U.H. and Uddin, M.N. 2022. Phytochemicals and *in-vitro* antioxidant activity analysis of *Aloe vera* by-products (skin) in different solvent extract. J. Agri. Food. Res. 10, 100460.

Ijaz, M., Abbas, S.N., Farooqi, S.H., Aqib, A.I., Anwar, G.A., Rehman, A. and Khan, A. 2018. Sero-epidemiology and hemato-biochemical study of bovine leptospirosis in flood affected zone of Pakistan. Acta. Tropica. 177, 51–57.

Jiang, X., Wang, Y., Qin, Y., He, W., Benlahrech, A., Zhang, Q. and Zheng, Y. 2017. Micheliolide provides protection of mice against *Staphylococcus aureus* and MRSA infection by down-regulating inflammatory response. Sci. Rep. 7(1), 41964.

Kishen, A., Shi, Z., Shrestha, A. and Neoh, K.G. 2008. An investigation on the antibacterial and antibiofilm efficacy of cationic nanoparticulates for root canal disinfection. J. Endodontics. 34(12), 1515–1520.

Lee, Y., Shin, D.H., Kim, J.H., Hong, S., Choi, D., Kim, Y.J. and Jung, Y. 2010. Caffeic acid phenethyl ester-mediated *Nrf2* activation and *IκB* kinase inhibition are involved in *NFκB* inhibitory effect: structural analysis for *NFκB* inhibition. Eur. J. Pharmacol. 643(1), 21–28.

Le Mandat Schultz, A., Bonnard, A., Barreau, F., Aigrain, Y., Pierre-Louis, C., Berrebi, D. and Peuchmaur, M. 2007. Expression of TLR-2, TLR-4, NOD2 and pNF-κB in a neonatal rat model of necrotizing enterocolitis. PLoS One 2(10), e1102.

Lin, S., Wu, H., Wang, C., Xiao, Z. and Xu, F. 2018. Regulatory T cells and acute lung injury: cytokines, uncontrolled inflammation, and therapeutic implications. Front. Immun. 9, 1545.

Lowy, F.D. 1998. *Staphylococcus aureus* infections. New. Eng. J. Med. 339(8), 520–532.

Ma, X., Guo, S., Jiang, K., Wang, X., Yin, N., Yang, Y. and Deng, G. 2019. MiR-128 mediates negative regulation in *Staphylococcus aureus* induced inflammation by targeting MyD88. Int. Immunopharmacol. 70, 135–146.

Moghaddasi, M.S. 2010. *Aloe vera* chemicals and usages. Adv. Environ. Biol. 4(3), 464–469.

O'Bryan, M.K., Gerdprasert, O., Nikolic-Paterson, D.J., Meinhardt, A., Muir, J.A., Foulds, L.M. and Hedger, M.P. 2005. Cytokine profiles in the testes of rats treated with lipopolysaccharide reveal localized suppression of inflammatory responses. Am. J. Physiol. Regul. Integ. Comp. Physiol. 288(6), R1744–R1755.

Oray, M., Abu Samra, K., Ebrahimiadib, N., Meese, H. and Foster, C.S. 2016. Long-term side effects of glucocorticoids. Expert. Opin. Drug. Saf. 15(4), 457–465.

Patel, T.P., Soni, S., Parikh, P., Gosai, J., Chruvattil, R. and Gupta, S. 2013. Swertiamarin: an active lead from *Enicostemma littorale* regulates hepatic and adipose tissue gene expression by targeting PPAR-γ and improves insulin sensitivity in experimental NIDDM rat model. Evid. Based. Complement. Alternat. Med. 2013, 358673.

Peinnequin, A., Mouret, C., Birot, O., Alonso, A., Mathieu, J., Clarençon, D. and Multon, E. 2004. Rat pro-inflammatory cytokine and cytokine related mRNA quantification by real-time polymerase chain reaction using SYBR green. BMC. Immunol. 5(1), 1–10.

Phua, J., Badia, J.R., Adhikari, N.K., Friedrich, J.O., Fowler, R.A., Singh, J.M. and Ferguson, N. 2009. Has mortality from acute respiratory distress syndrome decreased over time? A systematic review. Am. J. Res. Crit. Care. Med. 179(3), 220–227.

Pollitt, E.J., Szkuta, P.T., Burns, N. and Foster, S.J. 2018. *Staphylococcus aureus* infection dynamics. PLoS. Pathog. 14(6), e1007112.

Prince, L.R., Whyte, M.K., Sabroe, I. and Parker, L.C. 2011. The role of TLRs in neutrophil activation. Curr. Opin. Pharmaco. 11(4), 397–403.

Quispe, C., Mardones Leiva, L., Rapposell, S., Calina, D., Szopa, A. and Butnariu, M. 2021. Chitosan nanoparticles as a promising tool in nanomedicine with particular emphasis on oncological treatment. BMC 21(1), 318.

Ranjbar, R. and Yousefi, A. 2018. Effects of *aloe vera* and chitosan nanoparticle thin-film membranes on wound healing in full thickness infected wounds with methicillin resistant *Staphylococcus aureus*. Bull. Emerg. Trauma. 6(1), 8.

Reza Nazifi, S.M., Asgharshamsi, M.H., Dehkordi, M.M. and Zborowski, K.K. 2019. Antioxidant properties of *Aloe vera* components: a DFT theoretical evaluation. Free. Rad. Res. 53(8), 922–931.

Ricart, M.C., Rodríguez, S.M. and Duré, R.M. 2020. Laryngeal stent for acute and chronic respiratory distress in seven dogs with laryngeal paralysis. Open. Vet. J. 10(1), 4–10.

Rumbaugh, K.P., Colmer, J.A., Griswold, J.A. and Hamood, A.N. 2001. The effects of infection of thermal injury by *Pseudomonas aeruginosa* PAO1 on the murine cytokine response. Cytokine 16(4), 160–168.

Salem, S.S., Hammad, E.N., Mohamed, A.A. and El-Dougdoug, W. 2022. A comprehensive review of nanomaterials: types, synthesis, characterization, and applications. Biointerface. Res. Appl. Chem. 13(1), 41.

Silva, P., Guedes, D.F.C., Nakadi, F.V., Pécora, J.D. and Cruz-Filho, A.M.D. 2013. Chitosan: a new solution for removal of smear layer after root canal instrumentation. Int. Endodontic. J. 46(4), 332–338.

Sokołowska, M., Kowalski, M. and Pawliczak, R. 2005. Peroxisome proliferator-activated receptors-gamma (PPAR-gamma) and their role in immunoregulation and inflammation control. Postepy. Hig. Med. Dosw. 59, 472–484.

Solaberrieta, I., Jiménez, A. and Garrigós, M.C. 2022. Valorization of *Aloe vera* skin by-products to obtain bioactive compounds by microwave-assisted extraction: antioxidant activity and chemical composition. Antioxidants 11(6), 1058.

Suvarna, K.S., Layton, C. and Bancroft, J.D. 2018. Bancroft's theory and practice of histological techniques. Elsevier Health Sciences.

Sy, C.T., Davis, J.S., Eichenberger, E., Holland, T.L. and Fowler, V.G. 2015. *Staphylococcus aureus* infections: epidemiology, pathophysiology, clinical manifestations, and management. Clin. Microbiol. Rev. 28(3), 603–661.

Wang, H., Yu, G., Yu, H., Gu, M., Zhang, J., Meng, X. and Li, J. 2015. Characterization of *TLR2, NOD2*, and related cytokines in mammary glands infected by *Staphylococcus aureus* in a rat model. Acta. Vet. Scand. 57(1), 1–6.

Wong, M., Chowoenczyk, P. and Kirkham, B. 2005. Cardiovascular issues of COX-2 inhibitors and NSAIDs. Aust. J. Gen. Prac. 34(11), 945.

Xing, J., Moldobaeva, N. and Birukova, A.A. 2011. Atrial natriuretic peptide protects against *Staphylococcus aureus*-induced lung injury and endothelial barrier dysfunction. J. App. Phys. 110(1), 213–224.

Yahya, R., Al-Rajhi, A.M., Alzaid, S.Z., Al Abboud, M.A., Almuhayawi, M.S., Al Jaouni, S.K. and Abdelghany, T.M. 2022. Molecular docking and efficacy of *Aloe vera* gel based on chitosan nanoparticles against *Helicobacter pylori* and its antioxidant and anti-inflammatory activities. Polymers 14(15), 2994.

Yao, H., Sun, Y., Song, S., Qi, Y., Tao, X., Xu, L. and Peng, J. 2017. Protective effects of dioscin against lipopolysaccharide-induced acute lung injury through inhibition of oxidative stress and inflammation. Front. Pharmacol. 8, 120.

Yoshida, T., Shimada, K., Matsuura, K., Mandour, A.S., Hamabe, L., El-Husseiny, H.M. and Tanaka, R. 2022. Treatment of portal vein thrombosis using vascular access port implantation in a Dalmatian dog: a case report. Open. Vet. J. 12(3), 356–359.

Yuan, J.S., Reed, A., Chen, F. and Stewart, C.N. 2006. Statistical analysis of real-time PCR data. BMC. Bioinform. 7, 85.

Zhang, Z., Wang, Y., Shan, Y. and Yin, W. 2020. Acetylharpagide protects mice from *Staphylococcus aureus*-induced acute lung injury by inhibiting NF-κB signaling pathway. Molecules 25(23), 5523.

Zhou, Y., Yu, S., Wu, J., Chen, Y. and Zhao, Y. 2015. Sulfiredoxin-1 exerts anti-apoptotic and neuroprotective effects against oxidative stress-induced injury in rat cortical astrocytes following exposure to oxygen-glucose deprivation and hydrogen peroxide. Int. J. Mol. Med. 36(1), 43–52.

Zhu, Y., Hu, C., Zheng, P., Miao, L., Yan, X., Li, H. and Li, Y. 2016. Ginsenoside Rb1 alleviates aluminum chloride-induced rat osteoblasts dysfunction. Toxicology 368, 183–188.